Climate Dynamics (2025) 63:349
https://doi.org/10.1007/s00382-025-07833-2

ORIGINAL ARTICLE

Spatiotemporal trends of annual minimum sea surface temperature in the Eastern China seas

Wenxiang Ding[1] · Caiyun Zhang[2] · Yongxin Chen[1] · Jingrui Mo[1] · Rui Zeng[1] · Qiong Wu[1]

Received: 21 December 2024 / Accepted: 31 July 2025

Abstract

Minimum annual sea surface temperature (T_{min}) plays a critical role in shaping marine ecological processes, yet its spatial and temporal variability remains insufficiently understood in many regional seas. This study investigates the spatiotemporal trends of T_{min} and its timing in the Eastern China seas from 1985 to 2022. Results reveal distinct spatial patterns, with warming trends (~0.3 °C/decade) associated with northward-flowing warm currents, and significant cooling trends (up to −0.4 °C/decade) along coastal regions influenced by cold coastal currents. T_{min} and its timing were strongly correlated with preceding atmospheric conditions from December onward, including air temperature, wind components, and surface heat fluxes. These relationships enabled the development of an artificial neural network model capable of predicting T_{min} and its timing with lead times of one to two months. Ecologically, lower T_{min} values were associated with increased chlorophyll concentrations and a higher frequency of marine cold spells. These findings offer new insights into the mechanisms driving T_{min} variability and highlight its potential predictability, providing a basis for improving early warning systems and supporting ecosystem-based management in a changing climate.

Keywords Annual minimum sea surface temperature · Eastern China seas · Wind · Heat flux · Chlorophyll

1 Introduction

Climate change is projected to increase the frequency of extreme weather events, such as heatwaves, droughts, cyclones, and cold spells (Drijfhout et al. 2015; Schlegel et al. 2021). As a fundamental parameter in oceanography and climate science, sea surface temperature (SST) influences numerous physical, chemical, and biological processes in the marine environment (Li and He 2014; Yeh et al. 2017; O'Reilly and Zanna 2018). It plays a significant role in regulating heat exchange between the ocean and atmosphere, which affects weather patterns, global climate, and marine ecosystems (Karnauskas et al. 2021; Ganguly et al. 2024). Extreme temperature events can have profound impacts on marine biodiversity, fisheries, and coastal communities (Oliver et al. 2021; Schlegel et al. 2021), leading to such phenomena as coral bleaching, changes in species distributions, and the collapse of vital habitats (Smale et al. 2019; Schlegel et al. 2021; Smith et al. 2023). Therefore, understanding the dynamics and extremes of SST is essential to predicting and mitigating the effects of climate change on the oceans and the communities that depend on them.

While the effects of extreme warm events have received considerable attention, extreme cold events also have significant ecological impacts (Schlegel et al. 2017, 2021). These cold events can push marine species beyond their thermal limits, leading to changes in species distributions, alterations in community structures, and potential evolutionary adaptations (Parmesan 2006; Campbell-Staton et al. 2017). Although less prominent than heatwaves, cold events can be equally severe in certain regions (Lentini et al. 2001; Florenchie et al. 2004). Research on extreme cold events often focuses on marine cold spells (MCSs), periods when SST is significantly lower than climate-normal values (Schlegel et al. 2021; Li et al. 2024). Conversely, the annual minimum sea surface temperature (T_{min}), which represents the lowest temperature recorded in a given year, offers a direct measure

✉ Caiyun Zhang
cyzhang@xmu.edu.cn

[1] Marine Science and Technology College, Zhejiang Ocean University, Zhoushan 316022, China

[2] State Key Laboratory of Marine Environmental Science, College of Ocean and Earth Sciences, Xiamen University, Xiamen 361102, China

Published online: 03 September 2025

of extreme cold conditions. While MCSs provide insights into periods of anomalous cold compared to historical norms, T_{min} is valuable in studying the tolerance of marine organisms to extreme cold and the effects cold conditions have on marine ecosystems. Analyzing T_{min} enhances our understanding of the frequency, intensity, and ecological consequences of these cold events, contributing to our knowledge of their role in marine ecosystem dynamics.

The Eastern China seas, comprising the Bohai sea, Yellow sea, and East China sea, are a marginal sea system in the Western Pacific and are characterized by complex patterns of ocean circulation (Fig. 1). The region's winter circulation consists of warm northward-flowing currents such as the Taiwan Warm Current, Kuroshio, Yellow sea Warm Current, and Tsushima Warm Current, as well as cold southward-flowing coastal currents like the Zhe-Min Coastal Current, Bohai sea Coastal Current, Yellow sea Coastal Current, and West Korea Coastal Current (Guo et al. 2023). Spatial and temporal variations in upper ocean temperatures significantly influence the coastal climate and ecological environments, affecting fisheries and weather forecasting in surrounding countries (Cai et al. 2006; Wang et al. 2018). Recent research has confirmed a noticeable warming trend in the SST of the Eastern China seas over the past few decades (Tang et al. 2020; Wang et al. 2023), with winter warming occurring more rapidly than summer warming (Cai et al. 2016, 2017). This phenomenon is attributed to complex factors including monsoons, ocean advection, vertical mixing, and air–sea heat fluxes (Liu 2005; Liu and Zhang 2013; Cai et al. 2016, 2017). However, patterns of winter warming and their controlling mechanisms are not yet clearly defined. Investigating the warming patterns in the upper ocean of the Eastern China seas from new perspectives, such as T_{min}, may provide valuable insights.

The Eastern China seas, known for their high primary productivity, support extensive fishing and aquaculture operations, making them vital to China's economic development (Hu and Wang 2016; Yin et al. 2022). Although significant winter warming has been observed in many studies (Cai et al. 2016, 2017; Wang et al. 2023), others have suggested that enhanced coastal currents during the winter might lead to reduced SSTs (Zhang et al. 2020). These contrasting trends highlight the complexity of regional SST dynamics and underscore the need to better understand the mechanisms driving T_{min} variability and its ecological consequences.

Despite its ecological and environmental significance, the main drivers of T_{min} variability in the Eastern China seas remain poorly understood. Given the observed spatial heterogeneity and its close connection to cold-season dynamics, identifying the dominant factors influencing T_{min} is crucial. Moreover, the strong associations between T_{min} and preceding atmospheric conditions suggest a potential for predictive modeling. This study investigates the key atmospheric

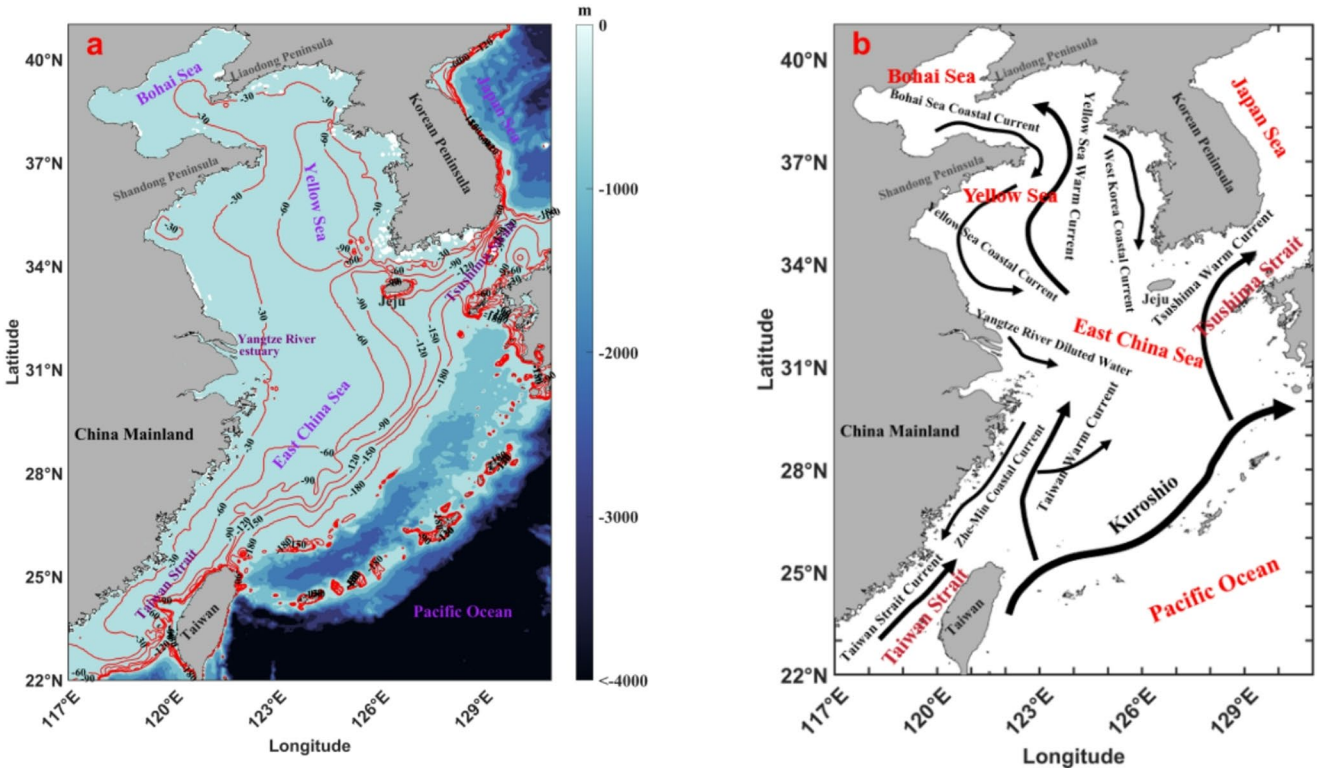

Fig. 1 Topography (**a**) and Currents (**b**) of the Eastern China seas

and oceanic drivers of T_{min}, assesses its predictability using an artificial neural network, and explores its implications for marine ecosystems. The findings are expected to improve understanding of regional cold extremes and contribute to early warning efforts and disaster risk reduction in marine environments.

2 Materials and methods

2.1 Data

The SST data used in this study were obtained from the Operational Sea Surface Temperature and Sea Ice Analysis (OSTIA) products, which have a spatial resolution of 0.05°. The OSTIA SST, which is a daily product provided by the UK Met Office, uses a variational assimilation algorithm that integrates microwave and infrared remote sensing data from multiple platforms with in situ measurements from the Global Telecommunications System (GTS) (Donlon et al. 2012). The data are corrected using ice concentration products from the Ocean and Sea Ice Satellite Applications Facility (EUMETSAT OSI-SAF), Advanced Along-Track Scanning Radiometer (AATSR) data, and buoy data, resulting in SST records that eliminate the effects of diurnal variation (Donlon et al. 2012). We collected SST data for the Eastern China Seas from 1985 to 2023, sourced from the European Copernicus program (http://marine.copernicus.eu). Previous studies have confirmed the consistency of OSTIA SST data with in situ measurements in this region (Wang et al. 2020). Although extending the analysis to earlier decades (e.g., 1960–1970s) could help provide a longer-term perspective, reliable and high-resolution SST datasets covering the Eastern China Seas are limited prior to 1985. In this study, we used the OSTIA reanalysis product, which begins in 1985, to ensure consistency in spatial and temporal resolution across the study period. This allows for robust spatiotemporal trend analysis while minimizing uncertainty associated with data quality and coverage in earlier periods.

Meteorological data were sourced from the National Centers for Environmental Prediction (NCEP), which has a spatial resolution of 0.3125° (~38 km). The NCEP provides various meteorological and oceanographic datasets, including forecasts, analyses, and climate products, supporting applications in weather prediction, climate research, and environmental monitoring. Generated using advanced numerical weather prediction models, the data are widely used for decision-making in research, policy, and industry (He and Zhao 2018; Zhu et al. 2021). We collected NCEP meteorological data from 1985 to 2023, including parameters such as air temperature at 2 m, wind (U and V) at 10 m, upward longwave radiation flux (Q_{ULW}), downward longwave radiation flux (Q_{DLW}), upward shortwave radiation flux (Q_{USW}), downward shortwave radiation flux (Q_{DSW}), latent heat flux (Q_{LH}), and sensible heat flux (Q_{SH}). These data were obtained from the Asia-Pacific Data-Research Center (http://apdrc.soest.hawaii.edu/data/data.php).

Daily chlorophyll (Chl) data were obtained from GlobColour, which produces data by merging satellite observations from SeaWiFS, MERIS, MODIS, VIIRS, and OLCI sensors and has a spatial resolution of 4 km. These datasets, covering the period from 1998 to 2023, are available through the Copernicus Marine Environmental Monitoring Service (CMEMS) at https://data.marine.copernicus.eu. The multi-sensor daily Chl product integrates Chl fields reconstructed using a consistent methodology for each sensor (Garnesson et al. 2019). Compared to the official products of the respective agencies, this integration significantly improves spatial coverage, which is important for both open ocean and coastal regions (Garnesson et al. 2019).

2.2 Calculation of annual minimum SST and decadal trends

The SST in the Eastern China Seas is characterized by pronounced seasonal fluctuations, and the lowest temperatures usually occur in winter (Bao and Ren 2014; Hu et al. 2022). However, the specific date on which the SST reaches its minimum can vary from year to year. Using the method of calculating annual maximum SST (T_{max}) outlined by Ding et al. (2024), we determined annual minimum SST (T_{min}), as shown in Fig. 2. Before calculating T_{min}, a 31 day moving average was applied to smooth the short-term fluctuations. Since T_{min} often occurs at the transition between years, a T_{min} recorded at the beginning of a year is attributed to the previous year. For example, if the lowest SST is observed in February 2017, it is considered the minimum for 2016.

Both air temperature and the meridional wind (V, where a northward wind is negative) also reach their annual minima in winter. The same methodology applied for SST was used to calculate the annual minimum air temperature ($AirT_{min}$) and its timing, as well as the annual minimum meridional wind component (V_{min}) and its timing.

To determine the decadal trends of T_{min} and its timing, we adapted a linear regression model to the yearly time series for each pixel, using T_{min} and T_{min} timing as dependent variables and year as the independent variable. The slopes of these regressions signify the rates of change for T_{min} (in °C/decade) and T_{min} timing (in days/decade). To assess the significance of the trends, we calculated the Pearson correlation coefficient (r) between the observed values and fitted values from the regression model. The Person correlation coefficient r, ranging between −1 and 1, measures the strength and direction of the linear relationship between

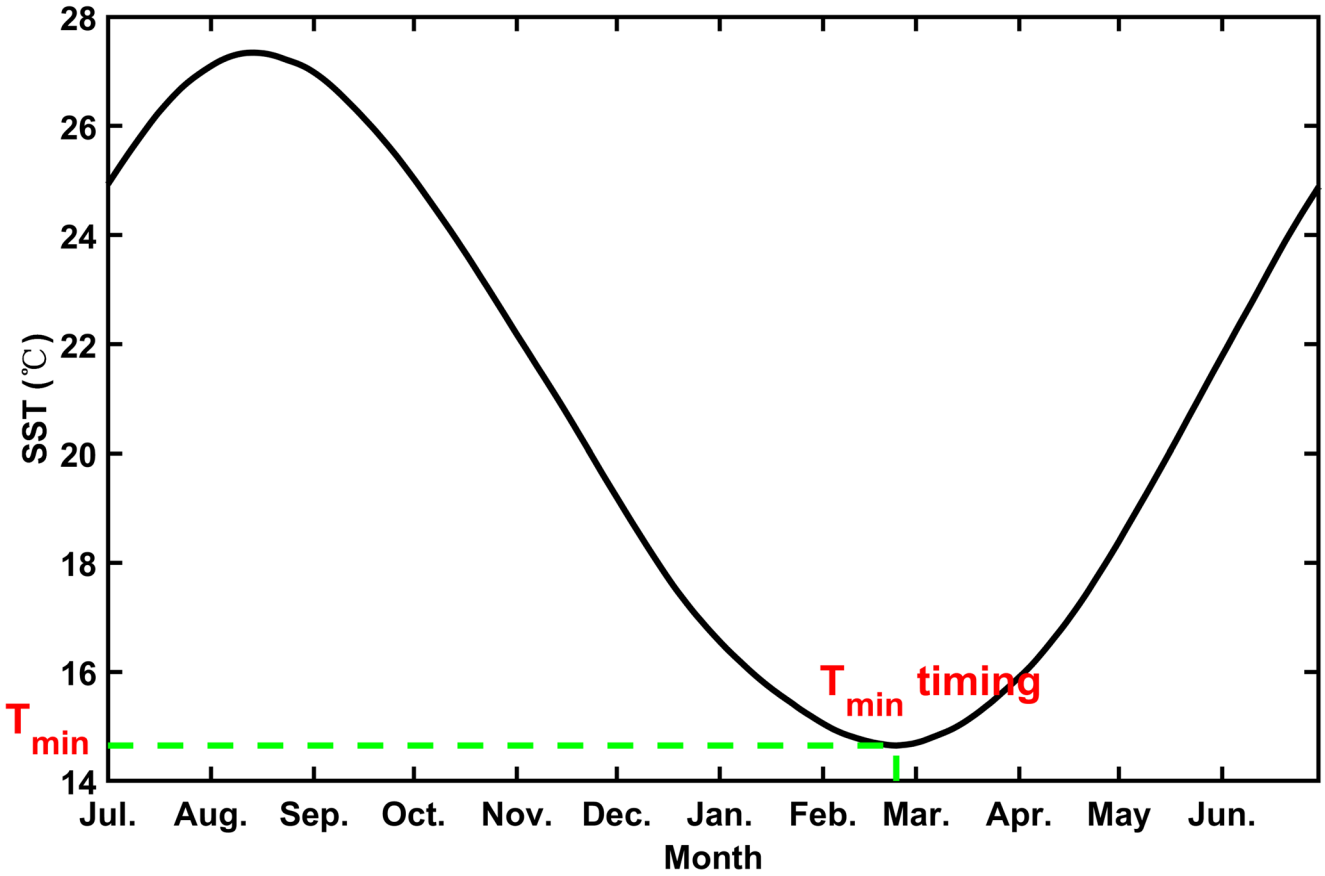

Fig. 2 Schematic diagram of T_{min} and its timing. The solid black line depicts the SST time series for a specific pixel over the course of a year

two continuous variables. The *t*-test was used to determine significance levels for the correlation, with $p<0.05$ indicating a significant correlation.

2.3 Calculation of Chl variability

To examine the impact of T_{min} on Chl variations, changes in Chl were calculated as follows: for each pixel, the average Chl value for the week preceding the T_{min} timing was designated as Chl_{pre}, and the average Chl value for the week following the T_{min} timing was designated as Chl_{fol}. The difference between these values ($\Delta Chl = Chl_{fol} - Chl_{pre}$) represents the fluctuation in Chl around the T_{min}. If the absolute value of ΔChl was less than 0.05 µg/L, Chl_{pre} and Chl_{fol} were considered not significantly different, and the pixel was excluded from further analysis. If ΔChl was greater than 0, it indicated an increase in Chl after the T_{min}, and the pixel was labeled as exhibiting a Chl increase. Conversely, if ΔChl was less than 0, it indicated a decrease in Chl after the T_{min}, and the pixel was labeled as exhibiting a Chl decrease. The net change in the number of pixels where Chl increased versus decreased was represented as $\Delta Pixels = N_{increase} - N_{decrease}$.

2.4 Calculation of marine cold-spells

MCSs are events where SST falls below a specific threshold established in previous studies (Schlegel et al. 2021; Walter et al. 2024). In this analysis, we identified MCSs for each pixel using daily OSTIA data. In particular, an MCS was defined as occurring when the daily SST fell below the 10th percentile of the climatological SST distribution, calculated on the basis of a 38 year dataset covering the years 1985–2022. To account for seasonal fluctuations, daily SST values were averaged over an 11 day window centered on each date, followed by a 31 day moving average for smoothing. An MCS event was considered contiguous if the temperature remained below the threshold for at least five consecutive days, allowing for gaps not exceeding three days. The MATLAB scripts used for this analysis are available at https://github.com/ZijieZhaoMMHW. The proportion of MCSs coincident with T_{min} timing was determined by comparing the number of pixels experiencing MCSs at the T_{min} timing with the total pixels in the study area.

2.5 Artificial neural network-based prediction of T_{min}

To investigate the predictability of T_{min} and its timing, we employed an artificial neural network (ANN) model using MATLAB. The network architecture consisted of a sequence input layer, followed by two fully connected layers with 16 neurons each. A dropout layer with a dropout rate of 0.5 was applied between the hidden layers to reduce overfitting. The final fully connected layer contained 1 neuron to produce the regression output, followed by a regression layer. The model was trained using the Adam optimizer with a learning rate of 0.001 for 500 epochs.

We adopted a leave-one-out cross-validation approach, treating each year as the test sample while the remaining years were used for training. Prediction performance was evaluated using the mean absolute error (MAE) between predicted and observed values. For comparison, the climatological mean over the 38 years was used as a baseline prediction. To evaluate the effectiveness of the ANN, a skill score was computed, representing the degree to which the model's MAE was reduced compared to the baseline climatological prediction.

$$\text{Skill score} = \left(1 - \frac{\text{MAE}_{\text{ANN}}}{\text{MAE}_{\text{CLI}}}\right) \times 100\%$$

Here, MAE_{ANN} and MAE_{CLI} represent the mean absolute errors calculated from the ANN predictions and the baseline climatological prediction, respectively.

3 Results

3.1 Spatial patterns and trends

Figure 3 show the spatial distributions of the mean T_{min} and its timing in the Eastern China Seas from 1985 to 2022. T_{min} exhibits a clear northwest–southeast gradient, with lower values in the northwestern regions and higher values in the southeastern regions. The T_{min} timing generally ranges from late January to mid-March, with earlier occurrences in the southern parts of the region. In particular, T_{min} occurs earlier in coastal areas, especially along the eastern coast of China and in the waters surrounding Taiwan Island. In contrast, T_{min} occurs later in the mid-northern East China Sea, the central Yellow Sea, and the western side of Jeju Island.

The spatial distributions of the correlation between T_{min} and its timing, as well as the trends in T_{min} timing, are shown in Fig. 4a and c. Regions with significant correlations or trends are scattered and localized. For example, a significant negative correlation between T_{min} and its timing is found in the central-northern Taiwan Strait, while a significant advancement in T_{min} timing is observed near the Yangtze River estuary. However, these significant areas are limited

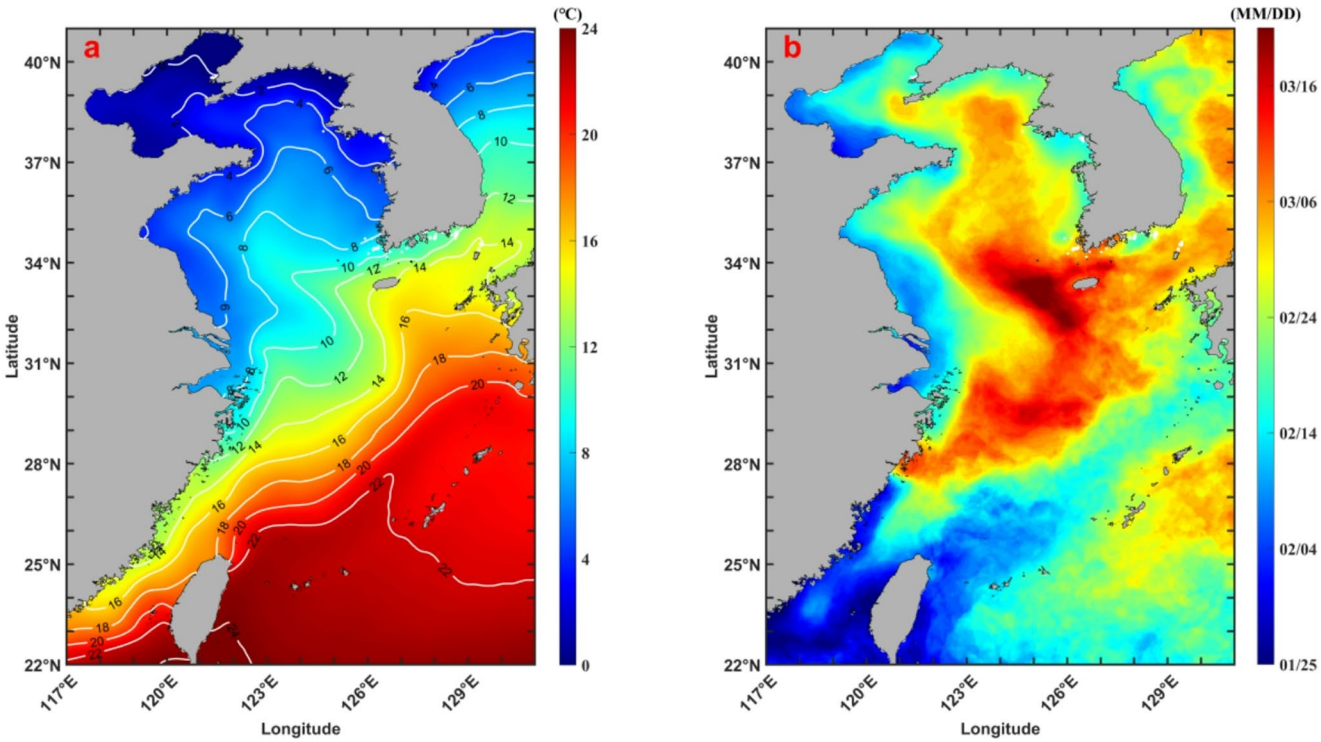

Fig. 3 Distribution of mean T_{min} (**a**) and T_{min} timing (**b**) across the Eastern China seas from 1985 to 2022

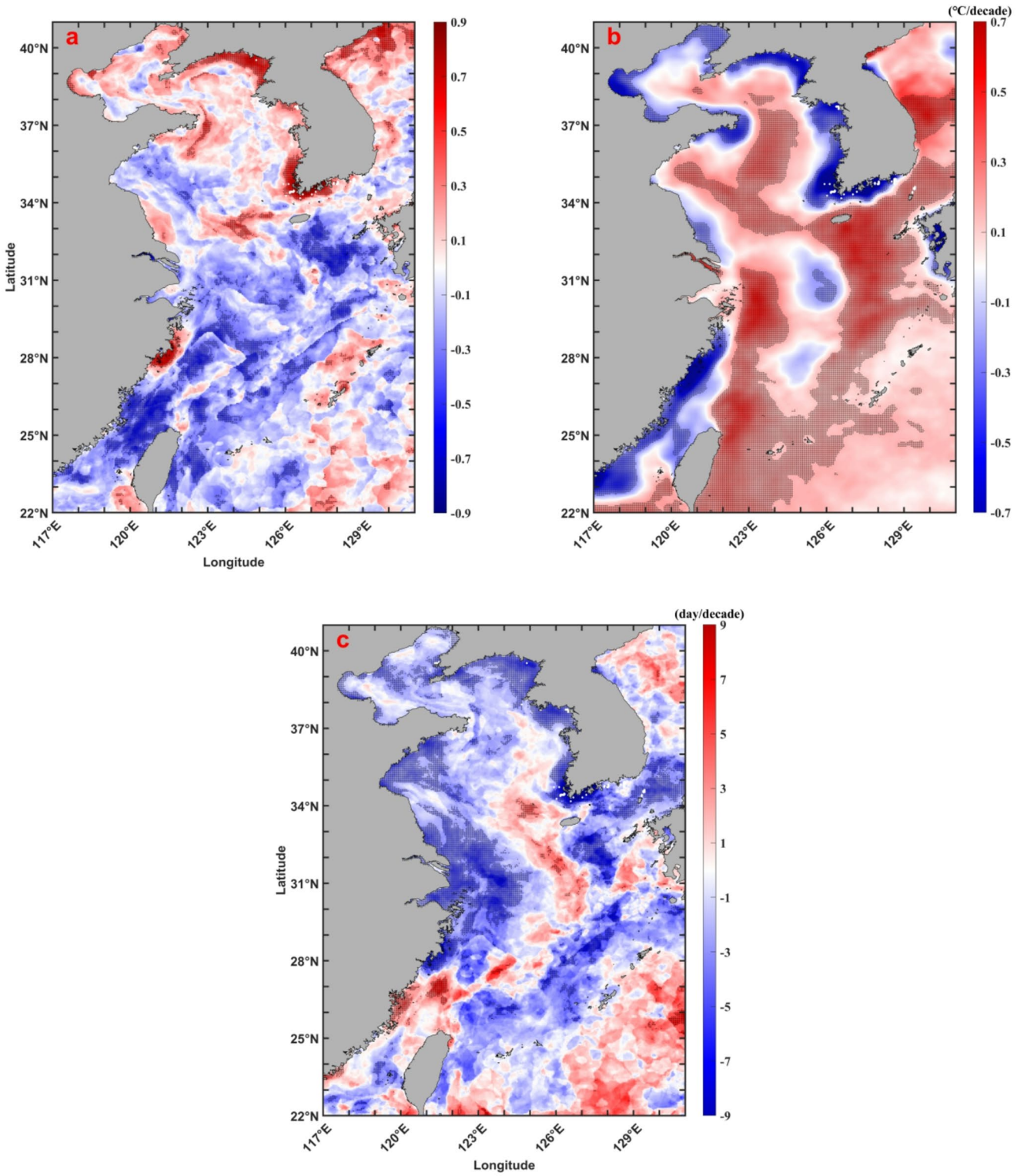

Fig. 4 Correlation coefficient (r) between T_{min} and T_{min} timing (**a**), decadal trend of T_{min} (°C/decade) (**b**), and decadal trend of T_{min} timing (days/decade) (**c**) across the Eastern China Seas. In (**a**), overlaid black dots indicate significant correlations, while in (**b**) and (**c**), overlaid black dots indicate significant trends

in spatial extent. Consequently, the area-averaged T_{min} and T_{min} timing for the entire study region are not significantly correlated, and the regional mean T_{min} timing shows no significant long-term trend (Fig. 5a).

In contrast, the spatial distribution of T_{min} trends reveals distinct boundaries between warming and cooling regions (Fig. 4b). Most coastal areas exhibit a significant cooling trend, with the exception of certain areas such as the coastal waters of the Japan Sea and the eastern coast of Taiwan Island. Offshore areas predominantly show significant warming trends, except for a few localized cooling zones in the central East China Sea. Despite the spatial extent of both warming and cooling regions, the area-averaged T_{min} across the entire study region does not show a significant trend (Fig. 5a). This is likely due to the opposing trends offsetting each other. When analyzed separately, significantly warming regions show an average increase of 0.3 °C/decade, while significantly cooling regions exhibit an average decrease of

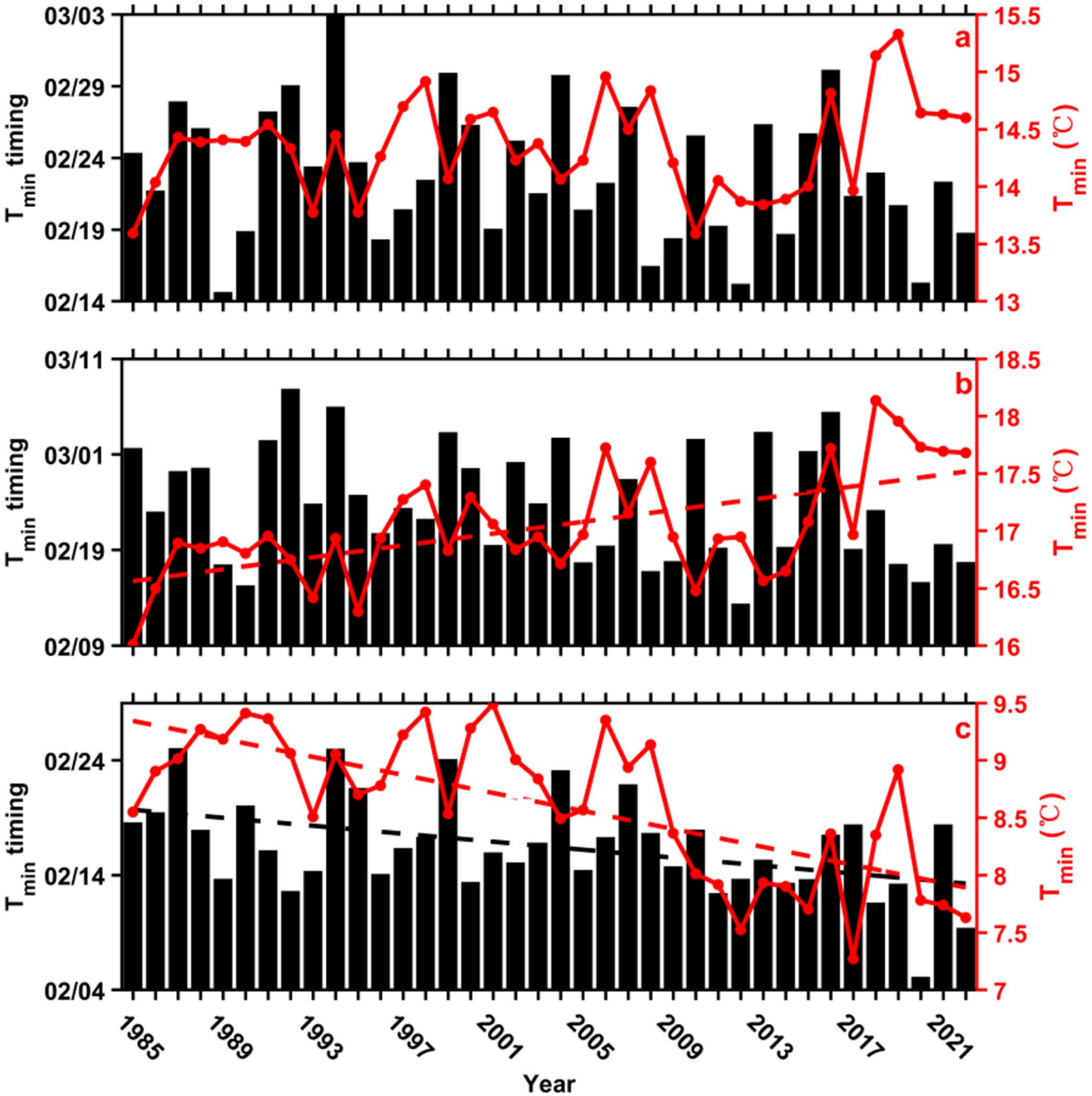

Fig. 5 Area-averaged time series of T_{min} (red lines) and T_{min} timing (black bars) from 1985 to 2022 for the Eastern China Seas (**a**), warming regions (**b**), and cooling regions (**c**) in the Eastern China Seas. The red dashed line represents the linear fit of the T_{min} time series considered significant, while the black dashed line represents the linear fit of the T_{min} timing time series considered significant

−0.4 °C/decade (Fig. 5b and c). Furthermore, the timing of T_{min} in the cooling regions has advanced significantly, at a rate of −1.7 days/decade (Fig. 5c).

3.2 Atmospheric and oceanic influences on T_{min}

The temporal evolution of atmospheric conditions and SST revealed a clear lag between air-based drivers and ocean response. In the Eastern China Seas, both air temperature and the meridional wind component (V) reached their minima during winter (Fig. 6a). On average, T_{min} occurred on February 17, approximately 25 days after the occurrence of the minimum air temperature ($AirT_{min}$; January 23), and 48 days after the minimum meridional wind (V_{min}; December 31). Despite this lag, significant correlations were observed among these variables. $AirT_{min}$ exhibited significant positive correlations with both the T_{min} in warming regions (WT_{min}) and cooling regions (CT_{min}), while V_{min} showed a significant correlation with CT_{min} (Fig. 6b, c). Additionally, the timing of $AirT_{min}$ and V_{min} was positively correlated with the timing of both WT_{min} and CT_{min} (Fig. 6d, e), indicating a consistent relationship between atmospheric minima and SST response.

Further analysis of monthly air temperature and wind components provided additional insights into the temporal associations (Table 1). In warming regions, WT_{min} was significantly influenced by the zonal wind component (U) in December. Specifically, weaker easterly winds (i.e., more negative U values) in December corresponded to higher WT_{min} values, as evidenced by a significant negative correlation between U and WT_{min}. In contrast, CT_{min} was more closely associated with V in December, where stronger northerly winds (more negative V values) were associated with lower CT_{min}, reflecting a significant positive correlation between V and CT_{min}.

The relationship between air temperature and WT_{min} was stronger and more persistent than that with CT_{min}. WT_{min} showed significant positive correlations with air temperature from December through March (Table 1), indicating that prolonged periods of elevated air temperature contribute cumulatively to higher T_{min} values in warming regions. In contrast, CT_{min} was mainly correlated with V and air temperature in December, with weaker correlations in other months (Table 1). Meanwhile, the timing of CT_{min} was most strongly influenced by air temperature and V in February (Table 1). Warmer air temperatures and weaker northerly winds in February were linked to an earlier occurrence of CT_{min}, indicating that short-term atmospheric conditions can significantly influence the timing of T_{min} in cooling regions.

Ocean-atmosphere heat fluxes were also found to be significantly related to T_{min} and its timing (Table 2). Longwave radiation fluxes (Q_{ULW} and Q_{DLW}) were significantly positively correlated with WT_{min} from December through March, highlighting their sustained role in moderating SST in warming regions. In contrast, in cooling regions, latent (Q_{LH}) and sensible (Q_{SH}) heat fluxes in December were significantly negatively correlated with CT_{min}. Higher values of Q_{LH} and Q_{SH}, indicating stronger heat loss from the ocean surface, were associated with lower T_{min}. Moreover, in February, Q_{LH} and Q_{SH} showed significant positive correlations with the timing of CT_{min}, suggesting that greater surface heat loss in this month tends to delay the occurrence of T_{min} in cooling regions.

Fig. 6 **a** Climatological time series from September to July for SST (black solid line), air temperature (red solid line), and V (blue solid line). The corresponding dashed lines in their respective colors indicate the times when SST, air temperature, and V reached their annual minimum values. **b** Scatter plot of $AirT_{min}$ and WT_{min} (blue hollow circles), and CT_{min} (red solid circles). **c** Scatter plot of V_{min} and WT_{min} (blue hollow circles), and CT_{min} (red solid circles). **d** Scatter plot of $AirT_{min}$ timing and WT_{min} timing (blue hollow circles), and CT_{min} timing (red solid circles). **e** Scatter plot of V_{min} timing and WT_{min} timing (blue hollow circles), and CT_{min} timing (red solid circles)

3.3 Relationship between T_{min} and Chl

To examine the response of Chl to T_{min}, we analyzed the weekly changes in Chl across 25 years (1998–2022), comparing values one week before and after T_{min} at each grid point (Fig. 7a). In 21 out of 25 years (84%), the net number of grid points with increasing Chl after T_{min} exceeded the number of grid points with decreasing Chl ($\Delta Pixels > 0$). Moreover, in 23 out of 25 years (92%), the area-averaged Chl change (ΔChl) was positive. These results indicate that an increase in Chl following T_{min} is a common phenomenon across the Eastern China Seas.

In addition, the magnitude and spatial extent of Chl changes were related to both T_{min} and its timing (Fig. 7b, c). T_{min} exhibited a significant negative correlation with ΔChl, indicating that lower T_{min} values were associated with greater increases in Chl. Furthermore, T_{min} timing showed significant positive correlations with both ΔChl and $\Delta Pixels$. In other words, when T_{min} occurred later in the season, both the number of grid points with increasing Chl and the magnitude of Chl increase tended to be higher.

Overall, these results demonstrate that in the Eastern China Seas, increases in Chl following T_{min} are widespread, and this response is more pronounced when T_{min} is lower and occurs later in the winter season.

3.4 Relationship between T_{min} and MCSs

A strong relationship was also observed between T_{min} and the probability of MCSs in the Eastern China Seas (Fig. 8).

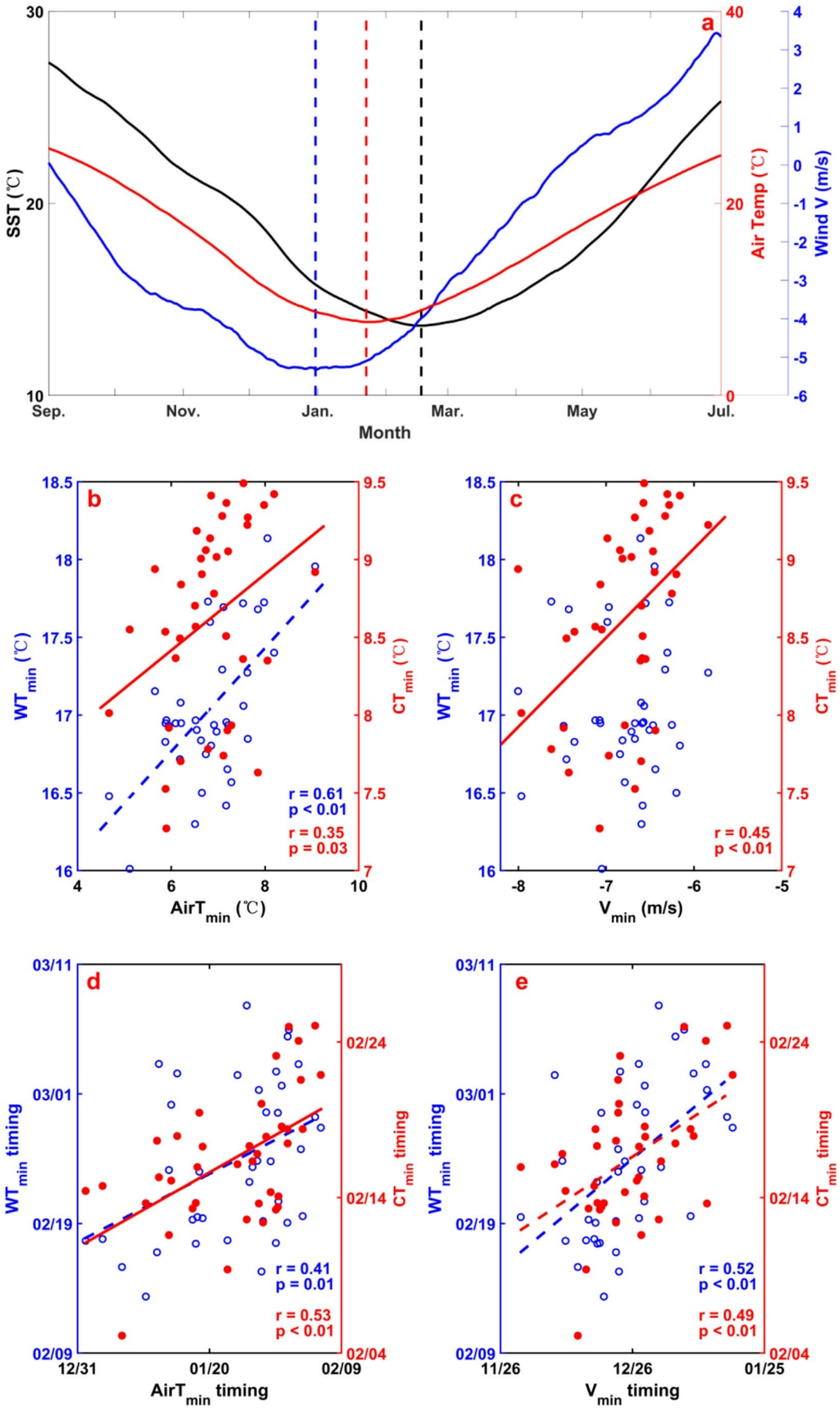
a
SST (℃)
Air Temp (℃)
Wind V (m/s)
Sep.
Nov.
Jan.
Mar.
May
Jul.
Month
b
WT$_{min}$ (℃)
CT$_{min}$ (℃)
r = 0.61
p < 0.01
r = 0.35
p = 0.03
AirT$_{min}$ (℃)
c
WT$_{min}$ (℃)
CT$_{min}$ (℃)
r = 0.45
p < 0.01
V$_{min}$ (m/s)
d
WT$_{min}$ timing
CT$_{min}$ timing
r = 0.41
p = 0.01
r = 0.53
p < 0.01
AirT$_{min}$ timing
e
WT$_{min}$ timing
CT$_{min}$ timing
r = 0.52
p < 0.01
r = 0.49
p < 0.01
V$_{min}$ timing

Table 1 Correlation coefficients ($n=38$) between monthly average wind components (U, V and wind speed [WS]) and air temperature (AT), and T_{min} and T_{min} timing from December to March

Month	Variable	T_{min}	T_{min} timing	WT_{min}	WT_{min} timing	CT_{min}	CT_{min} timing
December	U	−0.48***	−0.26	−0.45***	−0.18	−0.18	0.06
	V	0.21	0.27*	−0.01	0.33**	0.52***	0.27
	WS	−0.26	−0.24	0.03	−0.30*	−0.64***	−0.26
	AT	0.60***	0.41**	0.47***	0.34**	0.41**	0.19
January	U	−0.12	0.23	−0.25	0.34**	0.19	0.20
	V	0.17	−0.30*	0.09	−0.32*	0.10	−0.26
	WS	−0.25	0.09	−0.12	0.17	−0.18	0.15
	AT	0.69***	0.06	0.58***	−0.12	0.23	−0.11
February	U	−0.03	0.23	−0.20	0.22	0.24	0.27*
	V	0.41**	−0.48***	0.40**	−0.37**	0.19	−0.50***
	WS	−0.35**	0.28*	−0.28*	0.18	−0.28*	0.29*
	AT	0.67***	−0.39**	0.63***	−0.32**	0.27	−0.52***
March	U	−0.05	0.28*	−0.12	0.28*	0.19	0.12
	V	0.26	−0.40**	0.30*	−0.41**	−0.07	−0.29*
	WS	−0.30*	0.13	−0.21	0.08	−0.16	0.29*
	AT	0.62***	−0.37**	0.67***	−0.39**	−0.04	−0.44***

*** $p\leq0.01$, ** $p\leq0.05$, * $p\leq0.1$

Table 2 Correlation coefficients ($n=38$) between heat flux, T_{min}, and T_{min} timing from December through March

Month	Variable	T_{min}	T_{min} timing	WT_{min}	WT_{min} timing	CT_{min}	CT_{min} timing
Q_{ULW}	December	0.64***	0.29*	0.65***	0.17	0.16	0.07
	January	0.73***	0.25	0.67***	0.09	0.20	−0.02
	February	0.82***	−0.24	0.73***	−0.23	0.36**	−0.39**
	March	0.74***	−0.29*	0.77***	−0.32*	0.06	−0.46***
Q_{DLW}	December	0.56***	0.35**	0.45***	0.29*	0.33**	0.00
	January	0.59***	0.07	0.49***	−0.11	0.24	0.00
	February	0.44***	−0.42***	0.46***	−0.37**	0.11	−0.44***
	March	0.55***	−0.37**	0.44***	−0.40**	0.22	−0.20
Q_{USW}	December	−0.42***	−0.19	−0.27	−0.13	−0.32**	−0.04
	January	−0.38**	−0.05	−0.25	−0.00	−0.18	0.04
	February	−0.37**	0.06	−0.19	0.04	−0.32*	0.10
	March	−0.24	0.02	−0.02	−0.04	−0.38**	−0.04
Q_{DSW}	December	−0.29*	−0.07	−0.37**	−0.02	0.12	0.34**
	January	−0.28*	−0.08	−0.27	0.06	−0.14	−0.17
	February	0.07	0.11	−0.01	0.13	0.13	0.00
	March	−0.25	0.00	0.02	−0.00	−0.49***	−0.21
Q_{LH}	December	−0.26	−0.32**	0.07	−0.38**	−0.68***	−0.24
	January	−0.17	0.22	0.01	0.32**	−0.26	0.06
	February	−0.17	0.49***	−0.15	0.34**	−0.13	0.44***
	March	−0.20	0.33**	−0.10	0.32*	−0.11	0.14
Q_{SH}	December	−0.36**	−0.37**	−0.10	−0.40**	−0.61***	−0.27
	January	−0.39**	0.17	−0.26	0.31*	−0.22	0.14
	February	−0.35**	0.45***	−0.38**	0.32*	−0.13	0.55***
	March	−0.36**	0.46***	−0.42***	0.47***	0.13	0.33**

***$p\leq0.01$, ** $p\leq0.05$, * $p\leq0.1$

Across the study period, the average probability of MCSs occurrence was approximately 6.4%. However, at the time of T_{min}, this probability increased substantially to 14.3%, indicating that extremely low SSTs are associated with a heightened likelihood of MCSs events.

Furthermore, T_{min} was significantly negatively correlated with the probability of MCSs at T_{min} timing ($r=-0.89$, $p<0.01$). Lower T_{min} values were associated with a higher frequency of MCSs occurrence. Notably, the year 2010 exhibited the lowest T_{min} on record and the highest

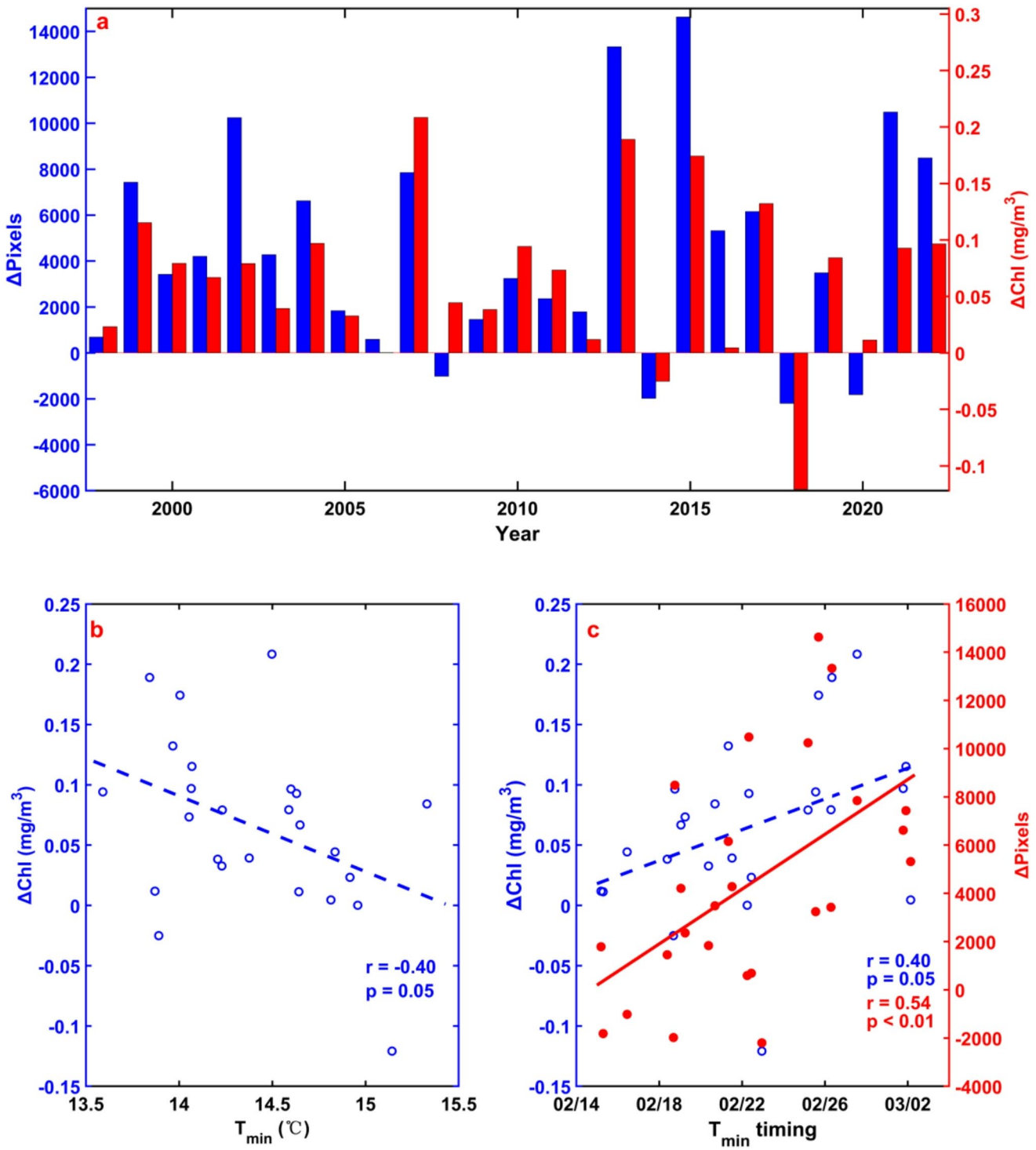

Fig. 7 **a** Annual time series of ΔPixels (blue bars) and ΔChl (red bars) in the Eastern China Seas. **b** Scatter plot of T_{min} verse ΔChl. **c** Scatter plot of T_{min} timing verse ΔChl (blue hollow circles) and ΔPixels (red solid circles)

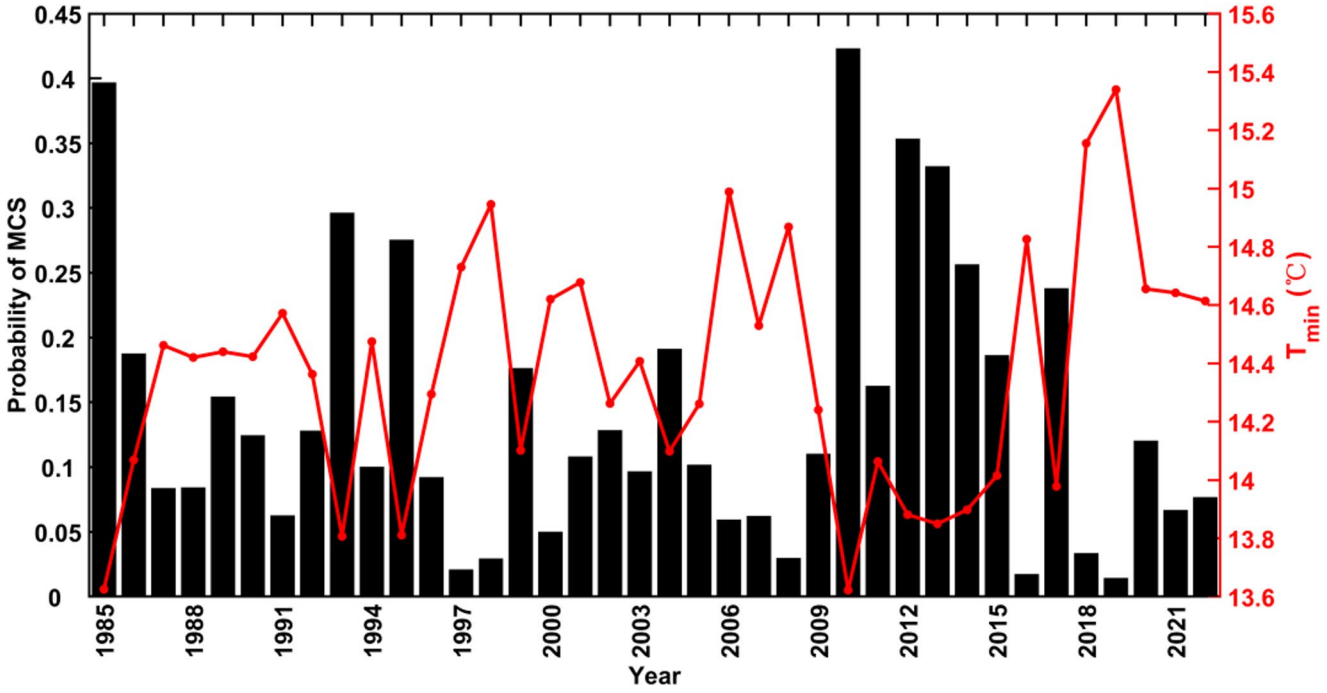

Fig. 8 Time series of the probability of MCSs at T_{min} timing

probability of MCSs (Fig. 8), with 42.3% of the study area experiencing MCSs when SST reached its minimum.

4 Discussion

4.1 Mechanisms of regional variability in T_{min}

As global climate warming continues (Bronselaer and Zanna 2020; Lyu et al. 2021), regional variations in SST have become increasingly important, with significant implications for marine ecosystems, local weather patterns, and fisheries (Wernberg et al. 2013, 2016). Previous studies have reported a general warming trend in winter SST across the Eastern China Seas (Yeh and Kim 2010; Cai et al. 2016, 2017). However, our results revealed pronounced spatial differences in the trends of T_{min}, with distinct boundaries separating warming and cooling regions (Figs. 4 and 5).

A comparison of Figs. 1b and 4b highlights a clear correspondence between T_{min} trend patterns and prevailing ocean currents. Warming regions are primarily associated with northward-flowing warm currents, particularly those linked to the Kuroshio and its branches, which transport warm water into the Eastern China Seas and elevate SST (Lian et al. 2016; Li et al. 2021; Tan et al. 2021; Cheng et al. 2025). In these regions, T_{min} exhibited a warming trend of approximately 0.3 °C/decade (Fig. 5b), consistent with the findings of Cai et al. (2016) and broadly aligned with global SST warming patterns.

In contrast, cooling regions are concentrated along coastal areas influenced by southward-flowing cold coastal currents. These areas exhibited a significant cooling trend in T_{min}, with rates reaching approximately −0.4 °C/decade (Fig. 5c), diverging sharply from global warming trends. The southward-flowing coastal currents has shown a strengthening trend in recent decades (Zhang et al. 2020), which may contribute to the observed T_{min} cooling. Moreover, these coastal currents are aligned with the prevailing northeasterly monsoon winds during winter (Sun et al. 2016; Yin et al. 2018). December, in particular, is characterized by the strongest northerly winds over the Eastern China Seas (Fig. 6a), which have significantly intensified over the 38 years (data not shown). This strengthening of the monsoonal winds has enhanced the southward transport of cold water, further amplifying the decreases in T_{min}.

Atmospheric processes further modulate SST variability through both direct heat exchange and ocean-atmosphere coupling (Sun et al. 2018; Gao et al. 2022). In warming regions, T_{min} exhibited significant positive correlations with air temperature and longwave radiation fluxes (Q_{ULW} and Q_{DLW}) from December through March (Tables 1 and 2), highlighting the cumulative influence of sustained atmospheric warmth on SST. The consistent correlation across multiple months suggests that ocean thermal inertia plays a crucial role in maintaining elevated T_{min} levels well into late winter.

In the cooling regions, the key factors influencing T_{min} can also be traced back to December (Tables 1 and

2). Stronger northerly winds, lower air temperatures, and enhanced sensible and latent heat fluxes in December contribute to lower T_{min} values. However, the influence of these factors weakens markedly in January and February, likely due to increasing ocean thermal inertia, which moderates the immediate atmospheric forcing effects (Soldatenko and Yusupov 2019). T_{min} in the cooling regions predominantly occurs in February (64%), and its timing is influenced by atmospheric conditions during that month. Weaker northerly winds, higher air temperatures, and lower sensible and latent heat fluxes tend to advance the timing of T_{min}. Interestingly, despite the absence of significant trends in February northerly wind strength, air temperature, or heat fluxes over the 38 year period, T_{min} timing has advanced significantly. This suggests that the observed advancement is likely driven by the combined or nonlinear effects of multiple factors, rather than changes in any single variable. A more detailed analysis would be required in future studies to fully understand these complex interactions.

In addition to ocean currents and atmospheric factors, vertical mixing, upwelling, and freshwater input from rivers also play significant roles in modulating SST in the Eastern China Seas (Kako et al. 2016; Hu and Wang 2016). Strong winter winds enhance vertical mixing, which brings colder, nutrient-rich subsurface waters to the surface, locally reducing SST and influencing T_{min}. Coastal upwelling, driven by wind and current dynamics, further contributes to localized cooling along the shoreline. Moreover, freshwater discharge from major rivers such as the Yangtze River affects surface stratification and temperature by introducing low-salinity water, which stabilizes the upper water column and alters the vertical heat distribution (Kako et al. 2016). Although these processes exhibit spatial heterogeneity and require further in situ observations for precise quantification, they likely contribute to the fine-scale SST variability and the sharp thermal gradients observed between warming and cooling regions.

While global SSTs generally show a warming trend, our results demonstrate that T_{min} trends in the Eastern China Seas are more complex, with distinct warming and cooling regions. This spatial contrast is closely linked to the unique geographical and oceanographic setting of the Eastern China Seas. The region is semi-enclosed, bordered by land to the west and north, and features a wide continental shelf (Fig. 1a) (Guo et al. 2023). On the eastern side, the warm Kuroshio intrudes into the Eastern China Seas, significantly influencing SST patterns (Lian et al. 2016; Bai et al. 2019). In winter, the enhanced East Asian Winter Monsoon strengthens cold coastal currents flowing southward along the coast, which cools the nearshore areas (Wei et al. 2014; Zhang et al. 2020). As a result, the interaction between the warm Kuroshio and the cold coastal currents creates sharp boundaries between warming and cooling zones in T_{min}. This complex interplay of topography, ocean currents, and monsoonal winds makes the Eastern China Seas a distinctive region for studying T_{min} variability and its ecological impacts.

Large-scale climate modes, such as the Arctic Oscillation (Zuo et al. 2016), North Atlantic Oscillation (Han et al. 2016), and El Niño-Southern Oscillation (Xie et al. 2024), are known to influence SST variability in the Eastern China Seas by modulating atmospheric circulation patterns and oceanic current systems. These climate modes can affect both the intensity and timing of cold air outbreaks, the strength of the East Asian Winter Monsoon, and the transport of warm or cold waters, thereby likely modulating both T_{min} and T_{min} timing. The potential nonlinear and lagged impacts of these large-scale modes on regional T_{min} variability merit further detailed investigation to better understand their role in shaping the observed spatial and temporal patterns.

4.2 Predictability of T_{min}

One of the key findings of this study is the strong linkage between T_{min} and preceding atmospheric conditions, which provides a valuable basis for enhancing its predictability. Air temperature and wind components exhibited significant correlations with both T_{min} and its timing, with many of these relationships traceable to atmospheric patterns established as early as December (Table 1). In particular, T_{min} showed strong correlations with $AirT_{min}$ and V_{min} across both warming and cooling regions, with T_{min} occurring on average 25 to 48 days later than these atmospheric minima (Fig. 6), highlighting the role of ocean thermal inertia.

Surface heat fluxes further enhanced this predictive framework. In warming regions, December longwave radiation fluxes showed strong positive correlations with T_{min}, while in cooling regions, T_{min} was more strongly influenced by December latent and sensible heat fluxes. Based on these findings, we developed an ANN model using 14 December variables as input to predict T_{min} and T_{min} timing. As shown in Table 3, the ANN achieved a MAE of 0.22 °C for T_{min} prediction in warming regions, which was notably lower than the MAE of 0.45 °C in cooling regions. For T_{min} timing, the average prediction error was about 4–5 days in warming regions and approximately 3 days in cooling regions. The smaller error in the latter is partly due to the lower temporal variability of T_{min} timing in cooling regions, as indicated by the much smaller MAE_{CLI} compared to warming regions.

In terms of skill score, the ANN model demonstrated higher predictability in warming regions than in cooling regions, and the prediction of T_{min} was generally more accurate than that of T_{min} timing (Table 3). This difference

Table 3 Prediction performance of the ANN model for T_{min} and T_{min} timing (1985–2022) using December variables as input

Variable	T_{min} (°C)	T_{min} timing (day)	WT_{min} (°C)	WT_{min} timing (day)	CT_{min} (°C)	CT_{min} timing (day)
MAE_{ANN}	0.22	3.81	0.22	4.81	0.45	3.16
MAE_{CLI}	0.34	3.41	0.36	5.15	0.53	3.22
Skill score	34%	10%	40%	6%	14%	2%

can be attributed to the more persistent influence of air temperature and longwave radiation in warming regions, where their effects can extend coherently from December through March. In contrast, T_{min} timing in cooling regions was more strongly influenced by February variables such as air temperature, northerly winds, Q_{LH}, and Q_{SH} (Tables 1 and 2). Since our model is based solely on December conditions, it does not capture the subsequent atmospheric evolution in January and February, limiting the accuracy of T_{min} timing predictions in cooling regions.

Nevertheless, the ability to forecast T_{min} and T_{min} timing one to two months in advance offers practical value, particularly for assessing the risk of extreme low-temperature events and their ecological impacts. To further improve forecast accuracy, future efforts could adopt a two-step prediction strategy: an initial estimate based on December conditions, followed by updates incorporating January and February data. In addition, while the current model focuses on regional mean predictions, future work may extend this approach to grid-level predictions across the study area, enabling more detailed spatial assessments.

4.3 Ecological responses to T_{min}

Our analysis revealed a clear ecological signal associated with T_{min} variability, particularly in relation to Chl dynamics. Over the past 25 years of satellite-derived observations, we found that in 84% of the years, the number of grid cells showing an increase in Chl following T_{min} exceeded those with decreases (Fig. 7a). Additionally, 92% of the years exhibited positive regional-average Chl anomalies after T_{min}, suggesting that the occurrence of T_{min} often marks the onset of enhanced phytoplankton growth in the Eastern China Seas.

The relationship between SST and Chl is inherently complex and shaped by multiple oceanographic and ecological factors (Anderson et al. 2012; Guallar et al. 2017). One of the key physical mechanisms involved is thermal stratification (Thompson et al. 2015). During winter, cooling of the sea surface increases surface density, leading to convective mixing that disrupts stratification. This vertical mixing, reinforced by strong winter winds, brings nutrients to the surface but can also suppress phytoplankton retention in the euphotic zone. Once T_{min} occurs and SST begins to rise, surface stratification re-establishes, allowing phytoplankton to remain in the illuminated surface layer. Combined with nutrient enrichment from earlier mixing, this creates favorable conditions for phytoplankton blooms (Anderson 1998; Dawson et al. 2018).

This transition helps explain the significant negative correlation between T_{min} and ΔChl observed in our study (Fig. 7b). Notably, lower T_{min} values were associated with stronger increases in Chl. One potential explanation involves ecological imbalances between phytoplankton and zooplankton. Studies suggest that lower temperatures may reduce zooplankton grazing rates more than they limit phytoplankton growth, allowing phytoplankton populations to proliferate (Taucher and Oschlies 2011; Behrenfeld et al. 2013). Thus, in years with lower T_{min}, phytoplankton may experience reduced top-down control at a time when physical conditions (e.g., re-stratification, light availability, and nutrient supply) are particularly conducive to bloom development.

We also found a significant positive correlation between T_{min} timing and Chl (Fig. 7c). Years with delayed T_{min} were often followed by higher Chl values. Light availability likely plays a key role in this pattern. In the ECSs, solar irradiance increases steadily from February through March (Chang and McClean 1997; Sourisseau et al. 2017). A later T_{min} often aligns with this seasonal increase in sunlight, thus enhancing phytoplankton growth once stratification is re-established. Moreover, delayed T_{min} is strongly associated with stronger northerly winds and lower air temperatures in February (Table 1)—conditions that promote deeper and more sustained winter mixing. This prolonged mixing phase could lead to greater nutrient accumulation in the surface layer, fueling stronger phytoplankton responses once the water column stabilizes.

While these explanations are plausible, it is important to recognize limitations in satellite-based Chl estimations, especially in turbid coastal waters where resuspended sediments can artificially inflate Chl readings (Chen et al. 2019). However, the consistency of observed patterns across spatial domains and temporal scales suggests that the detected signals are not solely artifacts. Future research incorporating in situ Chl and nutrient measurements will be essential for confirming the ecological mechanisms proposed here.

Finally, we explored the link between T_{min} and MCS events. MCSs, defined by anomalously low SSTs, are associated with significant ecological disruptions (Schlegel et al. 2021). Our findings revealed that the likelihood of MCSs occurrence more than doubled around the timing of

T_{min}. Furthermore, T_{min} values were negatively correlated with MCSs frequency (Fig. 8), indicating that years with lower T_{min} tend to experience more MCSs (Fig. 8). Given the known impacts of MCSs on marine organisms and ecosystem stability (Santos et al. 2016; Schlegel et al. 2017), understanding how T_{min} modulates their occurrence could support adaptive marine management and enhance ecosystem resilience to extreme cold events.

In addition to Chl dynamics and MCS occurrence, changes in T_{min} may also affect higher trophic levels and key ecological communities. For example, lower T_{min} and increased MCSs can cause thermal stress or habitat loss for temperature-sensitive species such as coastal benthic organisms and juvenile fish (Santos et al. 2016). These disturbances can alter food web structures and lead to cascading ecological consequences. Moreover, elevated Chl levels following T_{min} may influence zooplankton populations, thereby affecting the feeding conditions of fish larvae and other higher consumers. Such bottom-up effects, along with potential mismatches in the timing of primary and secondary production, warrant further investigation (Sigler et al. 2016). Future research should focus on how T_{min}-driven shifts in phytoplankton dynamics propagate through the marine food web, particularly under ongoing climate change.

4.4 Management implications and future directions

This study offers several practical insights for marine policy and management. First, the demonstrated predictability of T_{min} using early-winter atmospheric and oceanic indicators provides an opportunity to improve seasonal forecasting. Incorporating T_{min} forecasts into management strategies could help guide decisions in aquaculture, fishery closures, and the protection of sensitive species.

Second, the observed responses of Chl and MCSs to T_{min} variability highlight the importance of integrated monitoring systems that combine physical, chemical, and biological data. Such systems can support better assessments of ecosystem health and improve preparedness for ecological risks linked to T_{min} extremes.

However, some limitations should be noted. The use of satellite-derived Chl data introduces uncertainty in turbid coastal waters, and the relatively short observation period limits the analysis of long-term or nonlinear trends. Additionally, this study did not explore subsurface processes—such as mixed layer depth or nutrient supply—which may influence surface patterns.

Future work should focus on developing more comprehensive T_{min} prediction models by incorporating large-scale climate drivers. Expanding in situ observations—especially of Chl, nutrients, and vertical mixing—will help validate satellite-based results and improve understanding of underlying mechanisms. Research into T_{min}'s ecological effects across different habitats and trophic levels will also be key for advancing ecosystem-based management in the Eastern China Seas under climate change.

5 Summary

This study systematically investigated the spatiotemporal trends of the minimum annual sea surface temperature (T_{min}) in the Eastern China Seas over the period 1985–2022. Significant spatial and temporal patterns in T_{min} and its timing were identified, showing distinct regional variations.

Distinct boundaries between warming and cooling regions were identified. Cooling trends occurred primarily in areas influenced by southward-flowing coastal cold currents, while warming trends were observed along northward-flowing warm current paths. In the warming regions, T_{min} increased at a rate of approximately 0.3 °C/decade. Conversely, the cooling regions experienced a decrease in T_{min} at a rate of −0.4 °C/decade, with the timing of T_{min} advancing significantly by 1.7 days/decade.

The variability of T_{min} and its timing was closely linked to preceding atmospheric conditions, particularly air temperature, wind patterns, and surface heat fluxes starting from early winter (December). These strong correlations enabled the development of an ANN model that could predict T_{min} and its timing one to two months in advance with reasonable accuracy, especially in warming regions. The model's performance highlights the important role of ocean thermal inertia and atmospheric-ocean coupling in governing T_{min} dynamics.

Ecologically, T_{min} was found to be a critical indicator associated with phytoplankton dynamics, as lower T_{min} values and delayed T_{min} timing were both linked to enhanced Chl concentrations. Furthermore, T_{min} was strongly correlated with the frequency of MCS events, underscoring its value in assessing the risk of extreme low-temperature impacts on marine ecosystems.

Overall, this study improves our understanding of the complex regional processes controlling winter SST minima in the Eastern China Seas and demonstrates the potential for using atmospheric precursors to forecast T_{min} and related ecological responses. These findings provide a valuable scientific basis for climate impact assessments and adaptive management strategies in this ecologically and economically important marine region.

Acknowledgements The research is supported by the National Natural Science Foundation of China (No. 42406212; No. U22A20579), and the National Key Research and Development Program of China (No. 2022YFC3105300).

Data availability The SST and chlorophyll data are produced by CMEMS and are available at http://marine.copernicus.eu, and the meteorological data are produced by APDRC and available at http://apdrc.soest.hawaii.edu.

Declarations

Conflict of interest The authors declare that there are no conflicts of interest regarding the publication of this paper.

References

Anderson DM (1998) Physiology and bloom dynamics of toxic alexandrium species, with emphasis on life cycle transitions, physiological ecology of harmful algal blooms. NATO ASI Series, vol G41. Springer, Berlin, Heidelberg

Anderson DM, Alpermann TJ, Cembella AD, Collos Y, Masseret E, Montresor M (2012) The globally distributed genus alexandrium: multifaceted roles in marine ecosystems and impacts on human health. Harmful Algae 14:10–35. https://doi.org/10.1016/j.hal.2011.10.012

Bai HK, Hu HB, Yang XQ, Ren XJ, Xu HM, Liu GQ (2019) Modeled MABL responses to the winter Kuroshio SST front in the East China sea and yellow sea. J Geophys Res Atmos 124(12):6069–6092. https://doi.org/10.1029/2018JD029570

Bao B, Ren G (2014) Climatological characteristics and long-term change of SST over the marginal seas of China. Cont Shelf Res 77:96–106. https://doi.org/10.1016/j.csr.2014.01.013

Behrenfeld MJ, Doney SC, Lima I, Boss ES, Siegel DA (2013) Annual cycles of ecological disturbance and recovery underlying the Subarctic Atlantic spring plankton bloom. Glob Biogeochem Cycles 27:526–540. https://doi.org/10.1002/gbc.20050

Bronselaer B, Zanna L (2020) Heat and carbon coupling reveals ocean warming due to circulation changes. Nature 584(7820):227. https://doi.org/10.1038/s41586-020-2573-5

Cai RS, Chen JL, Huang RH (2006) The response of marine environment in the off shore area of China and its adjacent ocean to recent global climate change. Chin J Atmos Sci 30(5):1019–1033 (in Chinese with English abstract)

Cai RS, Tan HJ, Qi QH (2016) Impacts of and adaptation to interdecadal marine climate change in coastal China seas. Int J Climatol 36:3770–3780. https://doi.org/10.1002/joc.4591

Cai RS, Tan HJ, Kontoyiannis H (2017) Robust surface warming in offshore China seas and its relationship to the East Asian monsoon wind field and ocean forcing on interdecadal time scales. J Clim 30:8987–9005. https://doi.org/10.1175/JCLI-D-16-0016.1

Campbell-Staton SC, Cheviron ZA, Rochette N, Catchen J, Losos JB, Edwards SV (2017) Winter storms drive rapid phenotypic, regulatory, and genomic shifts in the green anole Lizard. Science 357(6350):495–498. https://doi.org/10.1126/science.aam5512

Chang FH, McClean M (1997) Growth responses of alexandrium minutum (Dinophyceae) as a function of three different nitrogen sources and irradiance. N Z J Mar Freshwat Res 31(1):1–7. https://doi.org/10.1080/00288330.1997.9516740

Chen XY, Zhang J, Tong C, Liu RJ, Mu B, Ding J (2019) Retrieval algorithm of chlorophyll-a concentration in turbid waters from satellite HY-1 C coastal zone imager data. J Coastal Res 90:146–155. https://doi.org/10.2112/SI90-018.1

Cheng YL, Wan SM, Robinson RS, Matsuzaki KM, Zhao DB, Shen XY, Zhai LN, Tang Y, Liu HL, Li AC (2025) The history of the Tsushima warm current since the middle miocene: co-evolution with the Kuroshio current and the Western Pacific warm pool. Earth Planet Sci Lett 661:119385. https://doi.org/10.1016/j.epsl.2025.119385

Dawson HRS, Strutton PG, Gaube P (2018) The unusual surface chlorophyll signatures of Southern ocean eddies. J Geophys Res: Oceans 123(9):6053–6069. https://doi.org/10.1029/2017JC013628

Ding WX, Wu Q, Chen YX (2024) Trends of maximum annual sea surface temperature in the Eastern China seas. Front Mar Sci 11:1452125. https://doi.org/10.3389/fmars.2024.1452125

Donlon CJ, Martin M, Stark J, Roberts-Jones J, Fiedler E, Wimmer W (2012) The operational sea surface temperature and sea ice analysis (OSTIA) system. Remote Sens Environ 116:140–158. https://doi.org/10.1016/j.rse.2010.10.017

Drijfhout S, Bathiany S, Beaulieu C, Brovkin V, Claussen M, Huntingford C, Scheffer M, Sgubin G, Swingedouw D (2015) Catalogue of abrupt shifts in Intergovernmental Panel on Climate Change climate models. Proc Natl Acad Sci 112 (43): E5777-E5786. https://doi.org/10.1073/pnas.1511451112

Florenchie P, Reason CJC, Lutjeharms JRE, Rouault M, Roy C, Masson S (2004) Evolution of interannual warm and cold events in the Southeast Atlantic ocean. J Clim 17(12):2318–2334

Ganguly I, Gonzalez AO, Karnauskas KB (2024) On the role of wind-evaporation-SST feedbacks in the subseasonal variability of the East Pacific ITCZ. J Clim 37(1):129–143. https://doi.org/10.1175/JCLI-D-22-0849.1

Gao Y, Kamenkovich I, Perlin N, Kirtman B (2022) Oceanic advection controls mesoscale mixed layer heat budget and Air–Sea heat exchange in the Southern ocean. J Phys Oceanogr 52(4):537–555. https://doi.org/10.1175/JPO-D-21-0063.1

Garnesson P, Mangi A, Fanton d'Andon O, Demaria J, Bretagnon M (2019) The CMEMS globcolour chlorophyll-a product based on satellite observation: multi-sensor merging and flagging strategies. Ocean Sci 15(3):819–830. https://doi.org/10.5194/os-15-819-2019

Guallar C, Bacher C, Chapelle A (2017) Global and local factors driving the phenology of alexandrium minutum (Halim) blooms and its toxicity. Harmful Algae 67:44–60. https://doi.org/10.1016/j.hal.2017.05.005

Guo JT, Pan HD, Cao RC, Wang JF, Lv XQ (2023) Multiple timescale variations in water transparency in the Eastern China seas over the period 1997–2019. J Geophys Res-Oceans 128:e2022JC019170. https://doi.org/10.1029/2022JC019170

Han Z, Wan LFF J.H (2016) The observational influence of the North Atlantic SST tripole on the early spring atmospheric circulation. Geophys Res Lett 43(6):2998–3003. https://doi.org/10.1002/2016GL068099

He WP, Zhao SS (2018) Assessment of the quality of NCEP-2 and CFSR reanalysis daily temperature in China based on long-range correlation. Clim Dyn 50:493–505. https://doi.org/10.1007/s00382-017-3622-0

Hu JY, Wang XH (2016) Progress on upwelling studies in the China seas. Rev Geophys 54(3):653–673. https://doi.org/10.1002/2015RG000505

Hu SQ, Zhang WJ, Geng X, Sun JR (2022) Dominant modes of interannual variability of winter fog days over Eastern China and their association with major SST variability. Clim Dyn 58(1–2):413–426. https://doi.org/10.1007/s00382-021-05915-5

Kako S, Nakagawa T, Takayama K, Hirose N, Isobe A (2016) Impact of Changjiang river discharge on sea surface temperature in the East China sea. J Phys Oceanogr 46(6):1735–1750. https://doi.org/10.1175/JPO-D-15-0167.1

Karnauskas KB, Zhang L, Amaya DJ (2021) The atmospheric response to North Atlantic SST trends, 1870–2019. Geophys Res Lett 48(2):e2020GL090677. https://doi.org/10.1029/2020GL090677

Lentini CAD, Podesta GG, Campos EJD, Olson DB (2001) Sea surface temperature anomalies on the Western South Atlantic from

1982 to 1994. Cont Shelf Res 21(1):89–112. https://doi.org/10.1016/S0278-4343(00)00077-7

Li YZ, He RY (2014) Spatial and Temporal variability of SST and ocean color in the Gulf of Maine based on cloud-free SST and chlorophyll reconstructions in 2003–2012. Remote Sens Environ 144:98–108. https://doi.org/10.1016/j.rse.2014.01.019

Li DW, Yu M, Jia YH, Steinke S, Li L, Xiang R, Zhao MX (2021) Gradually cooling of the yellow sea warm current driven by tropical Pacific subsurface water temperature changes over the past 5 Kyr. Geophys Res Lett 48(10):e2021GL093534. https://doi.org/10.1029/2021GL093534

Li CH, Sun WJ, Ji JL, Zhu YX (2024) Historical marine cold spells in the South China sea: characteristics and trends. Remote Sens 16(7):1171. https://doi.org/10.3390/rs16071171

Lian EG, Yang SY, Wu H, Yang CF, Li C, Liu JT (2016) Kuroshio subsurface water feeds the wintertime Taiwan warm current on the inner East China sea shelf. J Geophys Res-Oceans 121(7):4790–4803. https://doi.org/10.1002/2016JC011869

Liu QY, Zhang Q (2013) Analysis on long-term change of sea surface temperature in the China seas. J Ocean Univ China 12(2):295–300. https://doi.org/10.1007/s11802-013-2172-2

Liu QY, Xie SP, Li LJ, Maximenko NA (2005) Ocean thermal advective effect on the annual range of sea surface temperature. Geophys Res Lett 32(24):L24604. https://doi.org/10.1029/2005GL024493

Lyu KW, Zhang XB, Church JA (2021) Projected ocean warming constrained by the ocean observational record. Nat Clim Change 11(10):834. https://doi.org/10.1038/s41558-021-01151-1

O'Reilly CH, Zanna L (2018) The signature of oceanic processes in decadal extratropical SST anomalies. Geophys Res Lett 45(15):7719–7730. https://doi.org/10.1029/2018GL079077

Oliver ECJ, Benthuysen JA, Darmaraki S, Donat MG, Hobday AJ, Holbrook NJ et al (2021) Marine heatwaves. Ann Rev Mar Sci 13:313–342. https://doi.org/10.1146/annurev-marine-032720-095144

Parmesan C (2006) Ecological and evolutionary responses to recent climate change. Annu Rev Ecol Evol Syst 37(1):637–669. https://doi.org/10.1146/annurev.ecolsys.37.091305.110100

Santos RO, Rehage JS, Boucek R, Osborne J (2016) Shift in recreational fishing catches as a function of an extreme cold event. Ecosphere 7(6):e01335. https://doi.org/10.1002/ecs2.1335

Schlegel RW, Oliver ECJ, Wernberg T, Smit AJ (2017) Nearshore and offshore co-occurrence of marine heatwaves and cold-spells. Prog Oceanogr 151:189–205. https://doi.org/10.1016/j.pocean.2017.01.004

Schlegel RW, Darmaraki S, Benthuysen JA, Filbee-Dexter K, Oliver ECJ (2021) Marine cold-spells. Prog Oceanogr 198:102684. https://doi.org/10.1016/j.pocean.2021.102684

Sigler MF, Napp JM, Stabeno PJ, Heintz RA, Lomas MW, Hunt GL (2016) Variation in annual production of copepods, euphausiids, and juvenile Walleye Pollock in the southeastern Bering sea. Deep-Sea Res Part II-Top Stud Oceanogr 134:223–234. https://doi.org/10.1016/j.dsr2.2016.01.003

Smale DA, Wernberg T, Oliver ECJ, Thomsen M, Harvey BP, Straub SC et al (2019) Marine heatwaves threaten global biodiversity and the provision of ecosystem services. Nat Clim Change 9(4):306–312. https://doi.org/10.1038/s41558-019-0412-1

Smith KE, Burrows MT, Hobday AJ, King NG, Moore PJ et al (2023) Biological impacts of marine heatwaves. Annu Rev Mar Sci 15(1):119–145. https://doi.org/10.1146/annurev-marine-032122-121437

Soldatenko SA, Yusupov RM (2019) Estimating the influence of thermal inertia and feedbacks in the atmosphere-ocean system on the variability of the global surface air temperature. Izv Atmos Ocean Phy 55(6):591–601. https://doi.org/10.1134/S000143381906015X

Sourisseau M, Le Guennec V, Le Gland G, Plus M, Chapelle A (2017) Resource competition affects plankton community structure: evidence from trait-based modeling. Front Mar Sci 4(52):1–14. https://doi.org/10.3389/fmars.2017.00052

Sun JQ, Wu S, Ao J (2016) Role of the North Pacific sea surface temperature in the East Asian winter monsoon decadal variability. Clim Dyn 46(11–12):3793–3805. https://doi.org/10.1007/s00382-015-2805-9

Sun XG, Tao LF, Yang XQ (2018) The influence of oceanic stochastic forcing on the atmospheric response to midlatitude North Pacific SST anomalies. Geophys Res Lett 45(17):9297–9304. https://doi.org/10.1029/2018GL078860

Tan HJ, Cai RS, Yan XH, Li CH (2021) Amplification of winter sea surface temperature response over East China seas to global warming acceleration and slowdown. Int J Climatol 41(3):2082–2099. https://doi.org/10.1002/joc.6948

Tang YL, Huangfu JL, Huang RH, Chen W (2020) Surface warming reacceleration in offshore China and its interdecadal effects on the East Asia-Pacific climate. Sci Rep 10(1):14811. https://doi.org/10.1038/s41598-020-71862-6

Taucher J, Oschlies A (2011) Can we predict the direction of marine primary production change under global warming? Geophys. Res Lett 38:L02603. https://doi.org/10.1029/2010GL045934

Thompson PA, O'Brien TD, Paerl HW, Peierls BL (2015) Precipitation as a driver of phytoplankton ecology in coastal waters: a climatic perspective. Estuar Coast Shelf Sci 162:119–129. https://doi.org/10.1016/j.ecss.2015.04.004

Walter RK, Dalsin M, Mazzini PLF, Pianca C (2024) Compound marine cold spells and hypoxic events in a nearshore upwelling system. Estuarine, Coast Shelf Sci 300:108706. https://doi.org/10.1016/j.ecss.2024.108706

Wang YQ, Lin XP, Li ZG (2018) Upper-ocean temperature trends in the Eastern China seas during 1976–1996. J Oceanol Limnol 36(5):1527–1536. https://doi.org/10.1007/s00343-019-7278-y

Wang CQ, Li X, Zhang YF, Zu ZQ, Zhang RY (2020) A comparative study of three SST reanalysis products and buoys data over the China offshore area. Haiyang Xuebao 42(3):118–128. https://doi.org/10.3969/j.issn.0253-4193.2020.03.011

Wang F, Li XG, Tang XH, Sun XX, Zhang JL, Yang DZ et al (2023) The seas around China in a warming climate. Nat Rev Earth Environ 4(8):535–551. https://doi.org/10.1038/s43017-023-00453-6

Wei K, Xu T, Du ZC, Gong HN, Xie BH (2014) How well do the current state-of-the-art CMIP5 models characterise the climatology of the East Asian winter monsoon? Clim Dyn 43(5–6):1241–1255. https://doi.org/10.1007/s00382-013-1929-z

Wernberg T, Smale DA, Tuya F, Thomsen MS, Langlois TJ, de Bettignies T et al (2013) An extreme Climatic event alters marine ecosystem structure in a global biodiversity hotspot. Nat Clim Change 3(1):78–82. https://doi.org/10.1038/nclimate1627

Wernberg T, Bennett S, Babcock RC, de Bettignies T, Cure K, Depczynski M et al (2016) Climate-driven regime shift of a temperate marine ecosystem. Science 353(6295):169–172. https://doi.org/10.1126/science.aad8745

Xie YW, Zhang WJ, Hu SQ, Jianga F (2024) Seasonal reversal of ENSO impacts on SST in the East China Sea-Kuroshio region. J Clim 37(5):1797–1810. https://doi.org/10.1175/JCLI-D-23-0556.1

Yeh SW, Kim CH (2010) Recent warming in the yellow/east China sea during winter and the associated atmospheric circulation. Cont Shelf Res 30(13):1428–1434

Yeh SW, So J, Lee JW, Kim MJ, Jeong JI, Park RJ (2017) Contributions of Asian pollution and SST forcings on precipitation change in the North Pacific. Atmos Res 192:30–37. https://doi.org/10.1016/j.atmosres.2017.03.014

Yin M, Li X, Xiao ZN, Li CY (2018) Relationships between intensity of the Kuroshio current in the East China sea and the East Asian

winter monsoon. Acta Oceanol Sin 37(7):8–19. https://doi.org/10.1007/s13131-018-1240-2

Yin WB, Ma YZ, Wang D, He SY, Huang DJ (2022) Surface upwelling off the Zhoushan islands, East China sea, from Himawari-8 AHI data. Remote Sens 14(14):3261. https://doi.org/10.3390/rs14143261

Zhang CY, Huang Y, Ding WX (2020) Enhancement of Zhe-Min coastal water in the Taiwan Strait in winter. J Oceanogr 76:197–209. https://doi.org/10.1007/s10872-020-00539-5

Zhu X, Dong TY, Zhao SS, He WP (2021) A comparison of global surface air temperature over the oceans between CMIP5 models and NCEP reanalysis. Front Environ Sci 9:656779. https://doi.org/10.3389/fenvs.2021.65677

Zuo JQ, Ren HL, Wu BY, Li WJ (2016) Predictability of winter temperature in China from previous autumn Arctic sea ice. Clim Dyn 47(7–8):2331–2343. https://doi.org/10.1007/s00382-015-2966-6